COBEM 2021 26th International Congress of Mechanical Engineering
November 22-26, 2021, Virtual Congress, Brazil
ABCM Associação Brasileira de Engenharia e Ciências Mecânicas

COB-2021-XXXX
Wall Resolved Fluid-Structure Interaction Numerical Simulation of a Modern Wind Turbine Blade

Mohsen Lahooti
Department of Aeronautics, Imperial College, London, SW7 2AZ, United Kingdom
m.lahooti@imperial.ac.uk

Rodolfo C. Puraca
Department of Mechanical Engineering, Escola Politécnica - University of São Paulo - Brazil
rodolfo.puraca@usp.br

Bruno S. Carmo
Department of Mechanical Engineering, Escola Politécnica - University of São Paulo - Brazil
bruno.carmo@usp.br

Rafael Palacios
Department of Aeronautics, Imperial College, London, SW7 2AZ, United Kingdom
r.palacios@imperial.ac.uk

Spencer J. Sherwin
Department of Aeronautics, Imperial College, London, SW7 2AZ, United Kingdom
s.sherwin@imperial.ac.uk

Abstract. *Wall-resolved fluid-structure interaction (FSI) numerical simulations of the NREL 5 MW wind turbine blade model are carried out using two FSI approaches. The first method is based on high-fidelity Nektar++/SHARPy FSI framework, where the fluid governing equations are solved using high-order spectral/hp element method and the turbulent flow is resolved using Large Eddy Simulation (LES) on thick strips, while large-deformation dynamics of the structure are modelled using a geometrically-exact nonlinear composite beam finite-element model. Thick strip method for the fluid reduces the computational cost by considering a series of smaller domains, each of which has a finite thickness in the spanwise direction. Hence, the overall flow over the blade is treated with a sectional approach, where in each of these sections, strips, the 3D flow is reconstructed locally. Tip-loss correction is used to compensate for the sectional approach over the blade. The second FSI approach is based on OpenFoam/Calculix coupling, where the second-order unstructured finite volume method approach is used for solving the three-dimensional flow equations and the flow turbulence is captured using the k-ω SST model. The structural dynamics are modeled via second-order finite element method using standard solid elements. Effects of the solution fidelity on the prediction of aerodynamic forces as well as on the full three-dimensional flow modelling over the blade versus sectional representation of flow over the blade while incorporating the local three-dimensionality in each section and tip-correction are discussed. Further, significance of two approaches on modelling the slender blade, one using the beam mode and the other utilizing the full 3D solution of structure is addressed. Finally, assessment of convergence difficulties, computational cost and scalability of the two approaches are presented and discussed.*

Keywords: *Fluid-structure interaction, Large Eddy simulation, wind energy, wind turbine blades, aeroelasticity ....*

1. INTRODUCTION

Fluid-structure interaction (FSI) of slender, highly flexible structures in totally or partially separated turbulent flows has a broad application in aeroelastic simulation of high-altitude long-endurance (HALE) aircraft (Simpson and Palacios, 2013) and, aeroelastic and vortex-induced vibration (VIV) of wind turbine blades (Muñoz-Simón *et al.*, 2020; Horcas *et al.*, 2020) to name a few.

Numerical simulation of such FSI problems is computationally challenging, which is due to the high Reynolds number flow, large separation of boundary layer, and large deflection as well as high slenderness of the structure, where the major challenge is to accurately predict the aerodynamic forces on the deforming structure. A commonly used approach for such simulation is either using semi-empirical models (Facchinetti *et al.*, 2004; Gabbai and Benaroya, 2005) or using the

methods based on potential theory (Ramesh *et al.*, 2013; Katz and Plotkin, 2001; Simpson and Palacios, 2013) to predict the aerodynamic forces. However, despite their computational efficiency, the former might lack the predictable capability for new configurations that deviates noticeably from the experiment which the model is built upon, or as in the case of potential-theory-based approaches, lose the accuracy for the prediction of the fluid forces on the structure for flows with separation and finite boundary layer as well as the situation that involves vortex shedding and vortex interaction.

To address such shortcomings, higher-fidelity approaches that are based on the numerical solution of viscous Navier-Stokes equations such as Reynolds-averaged Navier-Stokes (RANS) or Large Eddy Simulation (LES) methods should be used for the prediction of fluid forces on the structure. RANS turbulence modelling is widely used for the simulation of turbulent flows and requires noticeably smaller computational resources compared to higher fidelity approaches such as the LES method. Therefore, the RANS based aeroelastic simulations can be used for the 3D simulations over the slender structures and are more suitable for industrial applications. However, such approaches are not accurate for flows that feature high turbulent intensity, massive separation or include dynamically moving bodies such as those encountered in the deep stall and VIV of turbine blades.

On the other hand, large eddy simulation of turbulent flow can address the aforementioned shortcomings of RANS methods and other approaches. However, it requires an extensive computational cost which can be prohibitively expensive for aeroelastic simulation of slender structures. A computationally efficient approach to address this challenge of LES simulations on high-aspect-ratio structures is to use the *thick strip* method proposed by (Bao *et al.*, 2016) for VIV of slender cylinders and further developed by (Lahooti *et al.*, 2021) for flexible wings in stall. In this method, the fluid domain is divided into a series of domains along the structure's spanwise length. Each *thick strip* is a three-dimensional domain perpendicular to the structure's local axis with a finite size thickness, where the spanwise thickness of the strips enables capturing local spanwise velocity correlations and reflecting the wake turbulence on structural dynamics. On the other hand, since the full $3D$ problems is represented by series of independent and locally $3D$ domains, the *thick strip* method provides a computationally efficient approach where LES can be used to get the resolved information of turbulence structures near the wall of high Reynolds number and massively separated flows.

In the present work, two different high-fidelity approaches are used for the simulation of high-aspect-ratio deformable structures with application to high aspect ratio wings and large wind turbine blades. The first approach is based on the *thick strip* LES method where the FSI solver is a coupling between Nektar++/SHARPy FSI solver (Lahooti *et al.*, 2021) while the second approach is based on the k-ω SST URANS turbulence modelling and FSI coupling between OpenFoam/CalculiX, using the software preCICE. The objective of the presented work is to provide a comparison between the two approaches for aeroelastic simulation of slender structures with high Re number and separated flows.

The rest of the paper is organised as follows: Sec. 2summarize the numerical approach used for the two FSI solvers, the results and discussions are presented in Sec. 3and finally Sec. 4concludes the work.

2. Numerical method

In the present work, two FSI solvers are developed and used for the fluid-structure interaction of a slender structure in high Re and separated flows. The first FSI solver is based on the coupling between Nektar++/SHARPy (Lahooti *et al.*, 2021) while the second FSI solver is a coupling between OpenFoam flow solver (OpenFoam, 1999) and CalculiX (Dhondt and Wittig, 1998) structural solver, using the software preCICE (Bungartz *et al.*, 2016). The numerical method and FSI coupling of each solver will be briefly introduced in this section.

2.1 *Nektar++/SHARPy* FSI framework: The *Thick-strip* LES FSI method

The *Nektar++/SHARPy* FSI framework (Lahooti *et al.*, 2021) is based on the *thick strip* method to provide an efficient computational framework for aeroelastic LES/DNS simulation of highly-flexible slender structure. In the *thick strip* method, the $3D$ fluid domain is divided into a series of independent domains along the structure's spanwise length L_s. Each strip is a three-dimensional domain consisting of two-dimensional x-y planes perpendicular to the structure's local axis which and has a finite size thickness of L_z in the spanwise direction, as shown schematically in Fig. 1. Having the spanwise thickness L_z for each strip enables capturing the local three-dimensional flow structures and hence the turbulent wake's local three-dimensionality. A distinct advantage of such an approach is that while the local $3D$ turbulence can be captured because of the thickness of the strips, only a fraction of a full three-dimensional fluid domain is modelled, which can be simulated efficiently. Hence, due to the reduced computational cost, using a more sophisticated approach such as LES or DNS becomes feasible to obtain the most resolved information near the structure.

In this FSI framework, the incompressible Navier-Stokes equations are discretized and solved for the fluid flow using the high-order spectral/hp method (Karniadakis and Sherwin, 2013). Since the structure undergoes large deformations, the Navier-Stokes equations are transformed and solved in non-inertial body-fitted coordinates to avoid dynamic remeshing during the solution procedure. Furthermore, the flow variables are assumed to be homogeneous in each strip with the periodic length equal to the strip thickness L_z, hence the Navier-Stokes equations can be discretized using Fourier approximation in the z-direction. On the other hand, using the Fourier approximation in the z-direction enables the Fourier

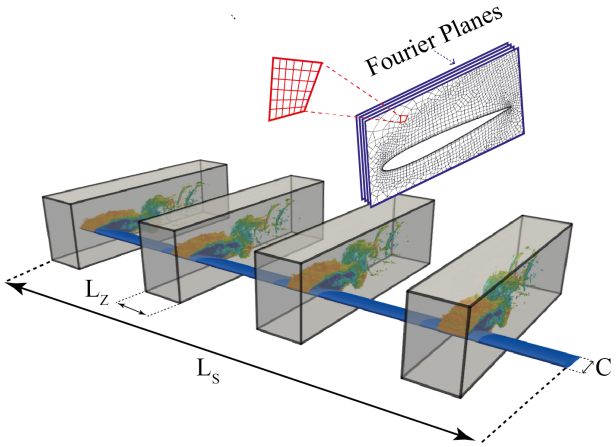

Figure 1. Schematic representation of the *thick strip* method. L_z and L_s are the spanwise length of the fluid strips and the structure length respectively. Fourier planes and a representative mesh in the x-y plane as well as a high-order element are also shown schematically.

transform of linear operators in the N.S. equations and decomposes the full 3D equations to sets of independent 2D equations. These 2D equations are then discretized in the x-y domain using spectral/hp method. The Fourier planes and spectral/hp elements for a fluid strip are shown schematically in Fig. 1.

The slender structure dynamics is modelled with a first-order approximation using a Geometrically-Exact Composite Beam (GECB) model and solved using the flexible multibody structural solver *SHARPy* with quadratic finite element method and Newmark-β time-integration(**?**Simpson, 2015). Finally, for the FSI coupling between the flow and structural solver, a loose coupling approach is adopted where the structural variables are first used to update the mesh in the N.S. equations, flow equations are solved and fluid forces are collected over the fluid strips and interpolated to the structural nodes where they are used to evolve the structural dynamics to the next time step. For the complete detail of the *Nektar++/SHARPy* FSI framework please refer to (Lahooti *et al.*, 2021).

2.2 OpenFoam/CalculiX FSI Solver

The OpenFoam/CalculiX FSI solver is a coupling between OpenFoam Flow solver (OpenFoam, 1999) and CalculiX (Dhondt and Wittig, 1998) solid solver. For the flow, the Reynolds-Averaged Navier-Stokes equations are discretized and solved using the second-order finite-volume method for space and the second-order backwards time integration for time. In addition, the PISO algorithm is used for the pressure-velocity coupling and k-ω SST method is used for turbulence modelling as well as the moving mesh approach is used to reflect the effect of deformation of the structure on fluid flow.

The structural dynamic is solved using the nonlinear $3D$ finite element dynamic solver of CalculiX (Dhondt and Wittig, 1998). Solid elements with orthropic materials are used to discretize the blade structure.

Loose coupling approach is adopted for the coupling between fluid and structural solvers where the preCICE (Bungartz *et al.*, 2016) is employed to transfer the information between OpenFoam and CalculiX as shown in Fig 2. PreCICE uses an OpenFoam adaptor (Chourdakis, 2017) to connect and gather information from OpenFoam, maps this information to the solid elements of CalculiX and transfer the data to the structural solver via a CalculiX adaptor (Uekermann *et al.*, 2017) (Fig. 22). Finally, it is worth mentioning that the nearest projection method is used in PreCICE for the mapping of forces and displacements between CalculiX and OpenFoam meshes due to its higher accuracy in comparison to the nearest neighbor method and its better performance in comparison with radial basis function approach.

3. Results and discussion

To demonstrate the FSI solvers and being able to provide a comparison across the two frameworks, we considered the static deformation of a cantilevered blade. To avoid the complexity arises from varying cross-section and twist along the span, a rectangular blade, i.e., constant cross section, is considered, and the NACA0012 airfoil is used for the blade cross-section. The structure length in the spanwise direction is set to $L_S^* = L_s/c = 16$ which is comparable to the NREL 5 MW wind turbine blade if the blade length is non-dimensionalized with chord length at the blade root. This problem has been analysed previously by (Patil and Hodges, 2004; Smith *et al.*, 2001; Simpson and Palacios, 2013; del Carre, 2020) using a lower-fidelity method, namely the unsteady lattice vortex method, which provides a means to validate our simulation results against other numerical approaches. The incoming flow with $U_\infty = 25$ m/s and density of $\rho_\infty = 0.08891\,\text{kg/m}^3$ is considered, which results in the chord-based Reynolds number of $Re_c = \rho_\infty U_\infty c/\mu = 1.56 \times 10^5$. Finally, the

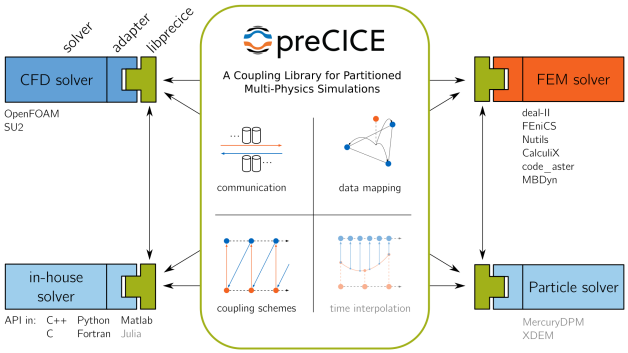

Figure 2. Schematic of coupling and flow of information in PreCICE. (Bungartz *et al.*, 2016)

Table 1. Structural properties of cantilevered blade

parameter	value (Simpson and Palacios, 2013)	non-dimensionalizaion	value
chord c	1 m	c^*	1
semi-span	$L_s = 16$ m	$L_s^* = L_s/c$	16
Elastic axis	$x_{ea} = 0.5c$	$x_{ea}^* = x_{ea}/c$	0.5
Center of gravity	$x_{gc} = 0.5c$	$x_{gc}^* = x_{gc}/c$	0.5
Mass per unit length	$\bar{m} = 0.75$ kg/m	$m^* = m/\left(\rho_\infty A_c\right)$	4.132
Moment of inertia	$J = 0.1$ kg $\cdot$ m	$J^* = J/\left(\rho_\infty c A_c\right)$	0.55
Torsional stiffness	$GJ = 1 \times 10^4$ Nm^2	$GJ^* = GJ/\left(\rho_\infty U_\infty^2 c^4\right)$	180
Bending stiffness	$EI_x = 2 \times 10^4$ Nm^2	$EI_x^* = EI_x/\left(\rho_\infty U_\infty^2 c^4\right)$	360
Chordwise bending stiffness	$EI_y = 5 \times 10^6$ Nm^2	$EI_y^* = EI_y/\left(\rho_\infty U_\infty^2 c^4\right)$	8.998×10^4

gravitational acceleration of $g = 9.754\,\text{m/s}^2$ is used in our simulations to have a similar condition with other published works and being able to compare the results.

As described earlier, the *Nektar++/SHARPy* FSI solver uses the *thick strip* approach where for this simulation. 8 strips with the spanwise length of $L_z^* = L_z/c = 1$ are used and distributed evenly over the blade span (Fig. 3). For each strip, 24 Fourier planes are used to discretize the L_z where each of these planes is a rectangular $2D$ (x, y) plane perpendicular to the local axis of the structure. Domain dimension and boundary conditions as well as the mesh used for *Nektar++/SHARPy* FSI are summarised in Fig. 3(b) and Fig. 3(c) respectively. On the other hand, the OpenFoam/CalculiX solver models the flow in the full $3D$ domain (Fig. 3(d)) where the domain in the x-y plane has the same dimension as that used in the *Nektar++/SHARPy* solver (Fig. 3(b)), while the third dimension extends $14c$ from the tip of the blade which results in a $30c$ of the domain in the z-direction (Fig. 3(d)). The computational grid used in OpenFoam simulation with a zoomed view of the mesh near the airfoil is depicted in Fig. 3(e) as well. Finally, the total mesh used for *Nektar++/SHARPy* consists of 27 million degrees of freedom with $y^+ < 1$ over the airfoil wall while for the OpenFoam/CalculiX solver, mesh consists of 9.1 million cells with $y^+ \simeq 100$.

As regards to the structural simulation, the *Nektar++/SHARPy* models the slender structure as a Geometrically-Exact nonlinear composite beam, while the OpenFoam/CalculiX solver adopts a full $3D$ nonlinear finite element approach for structural dynamics. The properties of the structure are summarised in Tab. 1.

3.1 Flow over NACA0012 airfoil

The deformation of the blade is accompanied by continuous twist along the span which consequently changes the local angle of attack, α, experienced by the fluid at each cross section as will be shown in subsequent sections. On the other hand, the flow exhibits different characteristics as the angle of attack changes. Hence, to ensure the accuracy of flow simulations during the FSI coupling and provide a comparison between the LES and URANS flow solvers, the flow is simulated over a range of angles of attack $\alpha = [2^\circ - 20^\circ]$ over the NACA0012 airfoil where quasi-3D approach, i.e. using a single strip with $L_Z^* = 1$ is used in *Nektar++*, while for OpenFoam simulation the airfoil section is considered as $2D$.

At the small angle of attack, i.e. $\alpha = 4^\circ$, fluid features a confined separation region near the trailing edge with small vortices being shed from the trailing edge (Fig. 4(a)). The separation layer moves upward and toward the leading edge and grows thicker as α increases (Fig. 4(b)), until it reaches the point of maximum lift and enters the stall region where the flow separates from the leading edge (Fig. 4(c)). At angles of attack beyond the stall, the flow features a time-dependent separated region over the suction side of the airfoil, limited by a shear layer. The height of this separation bubble is

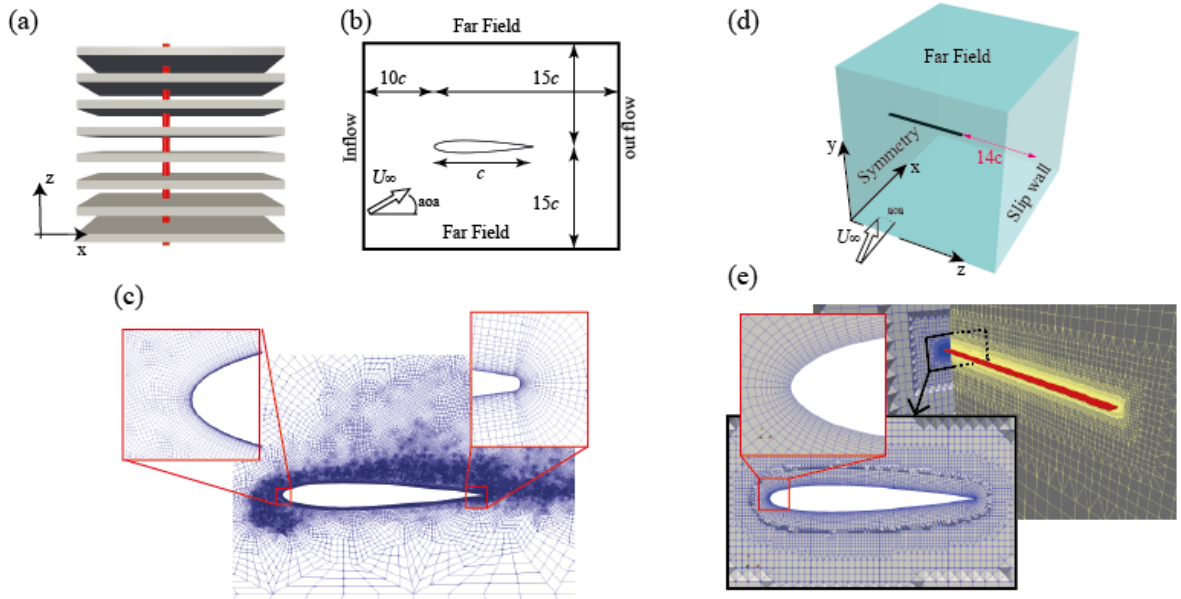

Figure 3. (a) Distribution of strips over the blade (b) Schematic of computational domain in the $x-y$ plane as well as the boundary conditions for both solver (c) Computational mesh with zoom view near leading and trailing edges of the airfoil for Nektar++ (d) Computational domain for OpenFoam (e) The grid used for flow solution in OpenFoam.

comparable to the chord length (Fig. 4(d)). As evident from this figure, both LES and URANS predict similar flow structures while, as expected, the LES simulation provides better resolved and finer turbulent structures (Fig. 4).

A more quantitative comparison of the results of the two solvers is provided in Fig. 5 in terms of the aerodynamic coefficients' polar. Both solvers predict correctly the trend of variation of aerodynamic coefficients and give a close prediction of these forces with a good agreement with the experimental data. The predicted forces from the URANS simulation are in better agreement than the LES simulation at angle of attack near the stall, Fig. 5(a), where the LES simulation overpredict the lift coefficient for $9^\circ < \alpha < 13^\circ$ [Fig. 5(a)]. However, the trend is recovered and good agreement with the experiment is regained for $\alpha \geq 16^\circ$. A possible reason for this over prediction of C_L near the stall could be due to the difference in the turbulence level of the freestream with experiments. Finally, it is worth noting that despite that URANS has a better prediction of C_L near the stall, the moment coefficient at the quarter of the chord, $C_M(c/4)$ has a noticeable deviation from the LES results and experimental data.

3.2 FSI simulation of cantilevered blade: Validation

In this section, the result of the FSI simulation of the blade will be presented and discussed. It should be mentioned here that at the time of writing, we have some technical difficulties with our OpenFoam/CalculiX FSI solver.

Despite the fact the mesh is adequate for rigid wing simulations, we were not able to converge the FSI simulations. When the wing started to deform, the flow speed at the trailing edge reached unreasonable high values and the calculation diverged. Besides that, the solid structural model was very expensive to solve, and we did not succeed scaling the simulation to run in more than one node.

Alternatives were tried to overcome the problem of the fluid solution diverging, such as a more refined adjustment of cell size transition between the upper and lower surfaces at the trailing edge of the wing, as well as a greater refinement of the first layer, aiming at not using a wall function model, but the error continued. Another attempt proposed was to add a damping term to the structural model of the wing to reduce the speed of deformation of the structure, reducing the excitation of the fluid solution and achieving a solution that did not diverge. The result of this modification only postponed

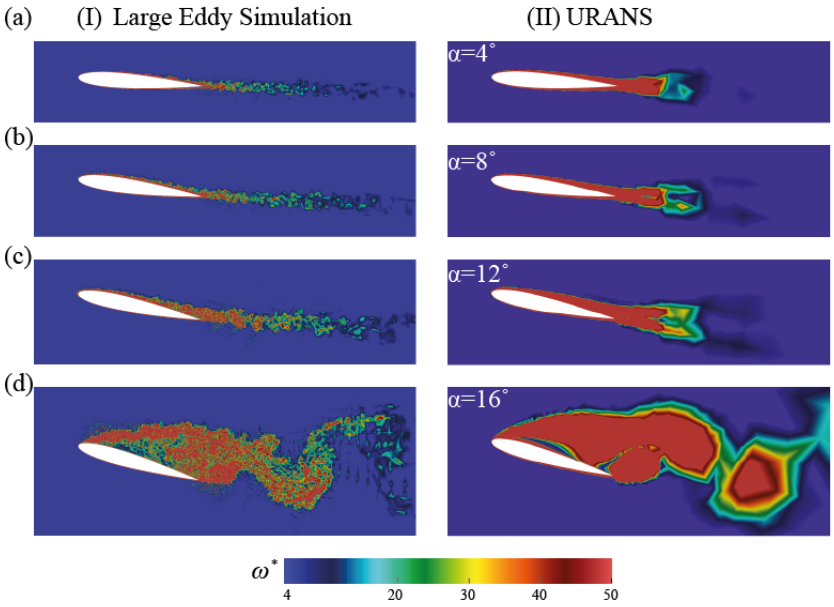

Figure 4. Contours of vorticity magnitude for LES and RANS simulations at various angles of attack over NACA0012 at $Re = 1.56 \times 10^5$.

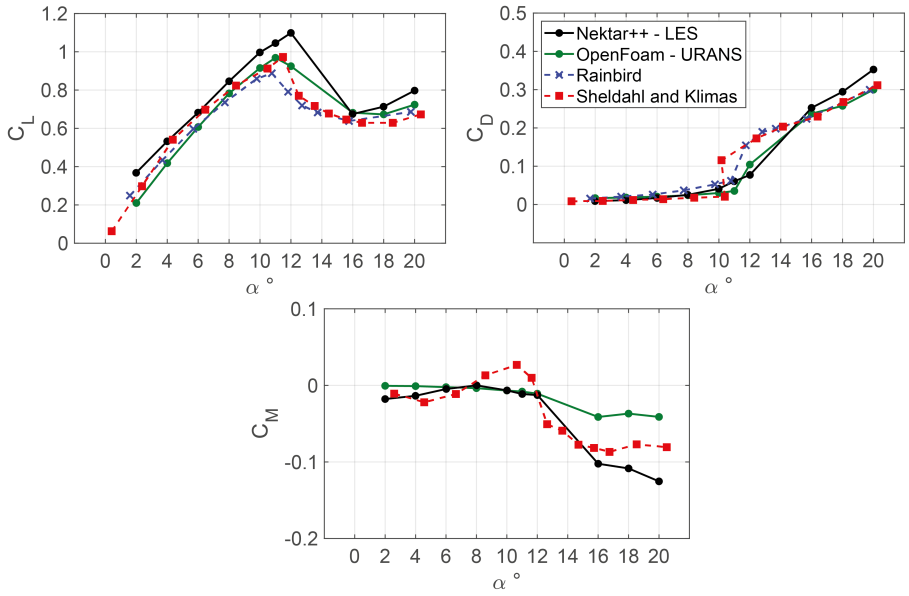

Figure 5. Variation of aerodynamic coefficient with angle of attack for $Re = 1.5 \times 10^5$ over NACA0012 (a) Lift coefficient (b) Drag coefficient. (c) Moment Coefficient around $c/4$. LES simulation (*Nektar++*): black solid lines, RANS simulation (OpenFoam):Green solid line, Experimental data from Sheldahl and Klimas (Klimas, 1981): Red dashed line, Experimental Data from Rainbird (Rainbird, 2016): Blue dashed line.

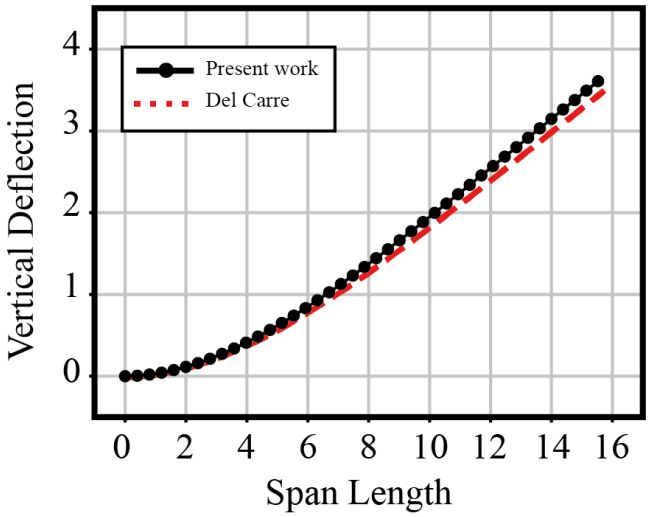

Figure 6. Vertical deflection of structure for flow with $Re = 1.56 \times 10^5$ and angle of attack of $\alpha_0 = 4°$. Black Solid lined with circles: *Nektar++/SHARPy* FSI using $N_s = 8$ strips along the span. Red dashed line: del Carre (2020) using *SHARPy* solver (del Carre *et al.*, 2019) with ULVM method for the prediction of aerodynamic forces.

the moment when the fluid solution diverged. As a last attempt, the coupling mode between OpenFOAM and CalculiX was modified in preCICE from explicit to implicit coupling, in which the solution of each timestep is re-iterated until the fluid and structure solution are converged within a tolerance. This method allows more stable coupling of highly transient problems, but it is much more computationally expensive than explicit coupling. The outcome of this modification resulted in a more stable solution, but this greater stability came from the fact that the wing structure deformed at a very lower speed, requiring a longer simulation time, reaching to the point of making this solution unfeasible, as in addition to being more computationally costly, would require more simulation time.

This shows that a more general approach to an FSI problem can be troublesome to use, due to problems related to the high computational cost and convergence challenges. Besides that, it might be very difficult to make general use, third-party software to perform well in high performance computing infrastructure. Therefore, only FSI results of *Nektar++/SHARPy* will be presented.

The computational domain and boundary conditions for the FSI problem are described in detail at the beginning of this section (Fig. 3) and the structural properties are provided in Tab. 1. To validate our simulation results, an incoming flow at an angle of attack $\alpha_0 = 4°$ is considered and, following del Carre (2020), gravitational acceleration is set to $g = 7.54\,\mathrm{m/s^2}$. First, the effect of the number of strips on the final wing deflection is tested with the number of strips $N_s = 4,\ 6,\ 8$ and 12 where the results for $N_s = 8$ and $N_s = 12$ showed less than 1% difference and Therefore, $N_s = 8$ is selected for the simulations.

Figure 6 shows the predicted deflection of the blade from *Nektar++/SHARPy* FSI simulation (black line) and compares it with the results of del Carre (2020) using the *SHARPy* solver with the unsteady vortex lattice (UVLM) method for the prediction of aerodynamic forces. Our result shows a close agreement with those from UVLM. Such good agreement between the results of our high-fidelity simulation with the lower-fidelity one for $\alpha = 4°$ is mainly due to the fact that at such a small angle of attack the boundary layer thickness is small over a large span of the structure. Hence, the viscous effects remain confined and can acceptably be handled with lower-fidelity approaches. It is worth mentioning that the structure undergoes a large vertical deformation about 22% of its initial length, which shows the robustness of our high-fidelity solver in handling such large deformations.

Before presenting the FSI result at a high angle of incident, the shortcoming of the *thick strip* approach on the global three-dimensionality and tip-loss effect should be addressed. The *thick strip* approach provides an efficient approach that enables LES/DNS FSI and aeroelasticity simulation of the slender structures for separated flows. However, since the fluid strips are implicitly connected via the structural dynamics and not directly interacting with each other, it cannot incorporate the global $3D$ effect such as the tip-loss effect. To overcome this problem, in our simulations, the tip-loss effect is considered via a correction factor in the form of Prandtl's tip loss factor correction fitted over the aerodynamic coefficients obtained from UVLM method. The resulting correction factor (Eq. (1)) is equal to 1 over the span except near the tip, where it gradually decreases to zero at tip. The aerodynamic forces calculated for each strip during the FSI coupling are multiplied by this correction factor and then interpolated to the structural nodes to update the new deformation state. The tip correction factor is as follows

$$F_{\text{tip}} = \frac{2}{\pi} \arccos\left(e^{-b\frac{1-s^*}{s^*}}\right) \tag{1}$$

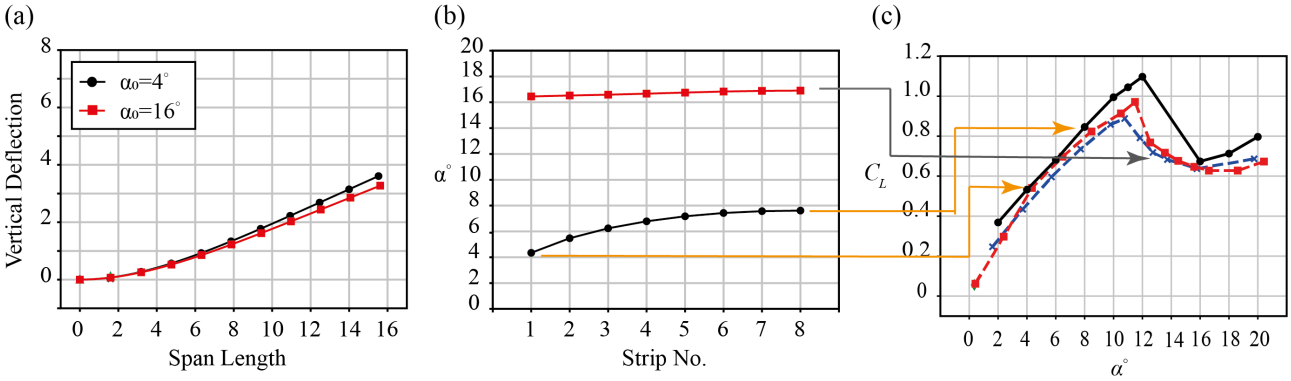

Figure 7. (a) Vertical deflection of structure for flows with $Re = 1.56 \times 10^5$ at angles of attack $\alpha_0 = 4°$ and $\alpha_0 = 16°$. (b) Variation of local angle of attack along the span. (c) C_L versus α for a single fluid strip from Fig. 5 repeated here for simplicity in analysis.

3.3 FSI simulation of cantilevered blade: Deep stall flow

In the previous section, the FSI result for a flow at a low angle of attack is presented and validated with low-fidelity approach results. In this section, we further extend our investigation for a flow with a large angle of attack. The strong point of the higher-fidelity methods (RANS, LES and DNS) for the prediction of aerodynamic forces lies in their ability to provide an accurate prediction of fluid forces for flows that experience large separation and finite thickness boundary layers. Hence, a flow with an incidence angle of $\alpha = 16°$ is considered and the resulting blade deflection is shown in Fig. 7(a), where the deflection of the blade under $\alpha = 4°$ is also included for the sake of comparison. It is evident from the figure that the blade undergoes a large deflection similar to the case with $\alpha = 4°$. However, despite the large angle of incidence of the flow with $\alpha = 16°$, the predicted deflection is slightly smaller than that of $\alpha = 4°$. This can be explained by examining the variation of local angle of attacks over the structural span as depicted in Fig. 7(b). For the flow with $\alpha = 4°$, as the blade deforms, the local angle of attack increases from $\alpha = 4°$ at the blade root to $\alpha = 8°$ near the tip. This change of angle of attack over the span results in the variation of the lift over the span from $C_L \simeq 0.5$ near the root to $C_L \simeq 0.85$ near the tip as indicated by the orange arrows in Fig. 7(c). However, for the flow with the $\alpha = 16°$, as the blade is completely submerged in the deep stall region, the angles of attack over the span does not change significantly and remains close to $16.5°$, which results in that the entire span of the blade experienced $C_L \simeq 0.7$, as shown with the black arrow in Fig. 7(c). Therefore, one can appreciate that the lift forces over the blade for $\alpha = 16°$ are approximately equal to the mean value of the lift that the blade experiences for $\alpha = 4°$, which explains the similar deflection of the blade for these two different flow regimes. It must be emphasised that, regardless of the amount of the structural deflection for the flow with $\alpha = 16°$, the FSI solvers based on the low-fidelity methods such as UVLM are not able to provide an accurate prediction of aerodynamic forces at such large angles of incidence due to the massive separation of the flow and finite thickness of the boundary layer.

Finally, Fig. 8 shows the deformed structure compiled with the flow strips where the Q criterion iso-contours are shown in each fluid strip and coloured by velocity magnitude.

4. Conclusion

In the present work, two high-fidelity fluid-structure interaction solvers is considered, where the first one is implemented in *Nektar++* framework, and is a coupling between *Nektar++* flow solver and *SHARPy* structural solver. This solver employed the *thick strip* approach which provides an efficient framework for LES/DNS FSI and aeroelastic simulations over slender structures. The second FSI solver is based on the OpenFoam/CalculiX coupling where the coupling is performed using the PreCICE library. This FSI solver uses the URANS turbulent modelling and hence has a lower fidelity compared with the *Nektar++/SHARPy* FSI solver. On the other hand, using the URANS turbulent modelling which requires less computational resources compared to LES simulations and hence, the OpenFoam/CalculiX solver can model the flow in a full $3D$ domain while the *Nektar++/SHARPy* FSI solver due LES modelling and the *thick strip* approach, treats the flow as quasi-3D simulations.

Flow over NACA0012 airfoil section at a wide range of angles of attack spanning from $\alpha = 2°$ to $\alpha = 20°$ is simulated and compared for the RANS and LES method. While both approaches provided a similar description of the flow field and boundary layer separation, the LES simulation provided a more resolved description of the turbulent flow as expected. The aerodynamic coefficients predicted with both approaches show good agreement with the experimental data. However, the lift coefficient predicted with the LES method is higher than the experimental data, which is most probably due to the

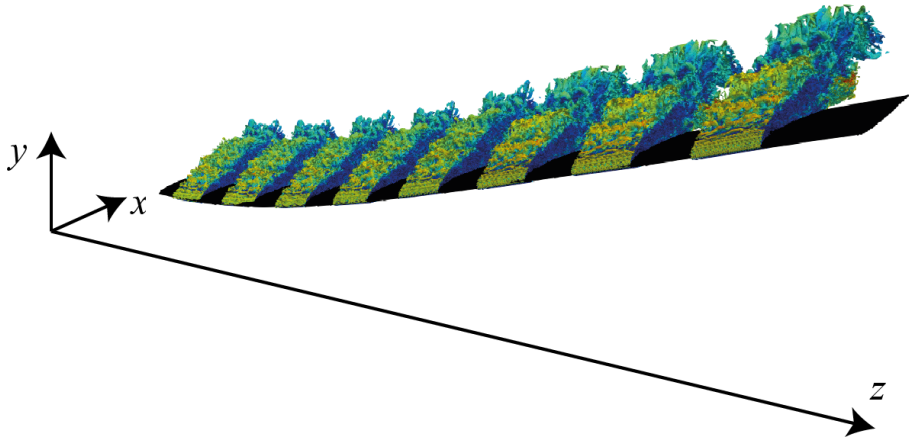

Figure 8. Q criteria iso-contour with $Q = 10$ colored by velocity magnitude over the deformed structure with flow Reynolds number $Re = 1.56 \times 10^5$ and initial angle of attack $\alpha_0 = 16°$. The contours range for velocity is in $[0 - 2]$ with blue color for lowest value and red corresponding to the highest value.

turbulence intensity of the incoming flow.

The FSI results of the *Nektar++/SHARPy* FSI solver are presented at two angles of attacks $\alpha = 4°$ and $\alpha = 16°$. The result for $\alpha = 4°$ validated against lower-fidelity approaches and shows an excellent agreement. Unfortunately, we were not able to converge the FSI simulations performed with OpenFoam/CalculiX due to technical difficulties.

Acknowledgments

This work is supported by European Commission (EC) under *H2020-EU.1.2.2.-FET Proactive* program and the Research and Innovation action (RIA) funding scheme, through the project *High Performance Computing in Wind Energy (HPCWE)* (grant agreement ID. 828799). ML, RP, and SJS also would like to thank EPSRC for the computational time made available on the UK supercomputing facility ARCHER via the UK Turbulence Consortium EP/R029326/1 and by the High Performance Computing facilities at Imperial College London. RCP and BSC would like to acknowledge the support from FAPESP (Fundação de Apoio à Pesquisa do Estado de São Paulo), Proc. 2019/01507-8, for this research. BSC acknowledges financial support from the Brazilian National Council for Scientific and Technological Development (CNPq) in the form of a productivity grant (grant number 312951/2018-3).

5. REFERENCES

Bao, Y., Palacios, R., Graham, M. and Sherwin, S., 2016. "Generalized thick strip modelling for vortex-induced vibration of long flexible cylinders". *Journal of Computational Physics*, Vol. 321, pp. 1079–1097.

Bungartz, H.J., Lindner, F., Gatzhammer, B., Mehl, M., Scheufele, K., Shukaev, A. and Uekermann, B., 2016. "preCICE – a fully parallel library for multi-physics surface coupling". *Computers and Fluids*, Vol. 141, pp. 250–258. ISSN 0045-7930. Advances in Fluid-Structure Interaction.

Chourdakis, G., 2017. *A general OpenFOAM adapter for the coupling library preCICE*. Ph.D. thesis, Technical University of Munich.

del Carre, A., 2020. *Aeroelasticity of very flexible aircraft at low altitudes*. Ph.D. thesis, Imperial College London.

del Carre, A., Muñoz-Simón, A., Goizueta, N. and Palacios, R., 2019. "Sharpy: A dynamic aeroelastic simulation toolbox for very flexible aircraft and wind turbines". *Journal of Open Source Software*, Vol. 4, No. 44, p. 1885.

Dhondt, G. and Wittig, K., 1998. "Calculix: A free software three-dimensional structural finite element program". URL `www.calculix.de`.

Facchinetti, M.L., De Langre, E. and Biolley, F., 2004. "Coupling of structure and wake oscillators in vortex-induced vibrations". *Journal of Fluids and structures*, Vol. 19, No. 2, pp. 123–140.

Gabbai, R.D. and Benaroya, H., 2005. "An overview of modeling and experiments of vortex-induced vibration of circular cylinders". *Journal of Sound and Vibration*, Vol. 282, No. 3-5, pp. 575–616.

Horcas, S.G., Barlas, T., Zahle, F. and Sørensen, N.N., 2020. "Vortex induced vibrations of wind turbine blades: Influence of the tip geometry". *Physics of Fluids*, Vol. 32, p. 065104.

Karniadakis, G. and Sherwin, S.J., 2013. *Spectral/hp element methods for computational fluid dynamics*. Oxford University Press.

Katz, J. and Plotkin, A., 2001. *Low-speed aerodynamics*, Vol. 13. Cambridge university press.

Klimas, R.E.S.P.C., 1981. "Aerodynamic characteristics of seven symmetrical airfoil sections through 180-degree angle of attack for use in aerodynamic analysis of vertical axis wind turbines". Technical report, Sandia National Labs., Albuquerque, NM (USA).

Lahooti, M., Palacios, R. and Sherwin, S.J., 2021. "Thick strip method for efficient large-eddy simulations of flexible wings in stall". In *AIAA Scitech 2021 Forum*. p. 0363.

Muñoz-Simón, A., Wynn, A. and Palacios, R., 2020. "Unsteady and three-dimensional aerodynamic effects on wind turbine rotor loads". In *AIAA Scitech 2020 Forum*. p. 0991.

OpenFoam, 1999. "Openfoam". URL `www.openfoam.com`.

Patil, M.J. and Hodges, D.H., 2004. "On the importance of aerodynamic and structural geometrical nonlinearities in aeroelastic behavior of high-aspect-ratio wings". *Journal of Fluids and Structures*, Vol. 19, No. 7, pp. 905–915.

Rainbird, J., 2016. *Blockage tolerant wind tunnel testing of aerofoils at angles of incidence from 0 to 360 degrees, with respect to the self-start of vertical-axis wind turbines*. Ph.D. thesis, Imperial College London.

Ramesh, K., Gopalarathnam, A., Edwards, J.R., Michael, V. and Granlund, K., 2013. "An unsteady airfoil theory applied to pitching motions validated against experiment and computation". *Theoretical and Computational Fluid Dynamics*, Vol. 27, No. 6, pp. 843–864.

Simpson, R.J. and Palacios, R., 2013. "Numerical aspects of nonlinear flexible aircraft flight dynamics modeling". In *54th AIAA/ASME/ASCE/AHS/ASC Structures, Structural Dynamics, and Materials Conference*. p. 1634.

Simpson, R.J.S., 2015. *Unsteady aerodynamics, reduced-order modelling, and predictive control in linear and nonlinear aeroelasticity with arbitrary kinematics*. Ph.D. thesis, Imperial College London.

Smith, M., Patil, M. and Hodges, D., 2001. "Cfd-based analysis of nonlinear aeroelastic behavior of high-aspect ratio wings". In *19th AIAA Applied Aerodynamics Conference*. p. 1582.

Uekermann, B., Bungartz, H., Yau, L., Chourdakis, G. and Rusch, A., 2017. "Official precice adapters for standard open-source solvers." *7th GACM Colloquium on Computational Mechanics for Young Scientists from Academia*.

6. RESPONSIBILITY NOTICE

All authors are responsible for the printed material included in this paper.